Traffic 2005; **6:** 548–561
Blackwell Munksgaard

doi: 10.1111/j.1600-0854.2005.00296.x

Brefeldin A Inhibits Circadian Remodeling of Chloroplast Structure in the Dinoflagellate *Gonyaulax*

Nasha Nassoury, Yunling Wang and David Morse*

Institut de Recherche en Biologie Végétale, Département de Sciences Biologiques, Université de Montréal, 4101 Sherbrooke est, Montreal, Quebec, Canada H1X2B2
**Corresponding author: david.morse@umontreal.ca*

Circadian increases in the rate of carbon fixation in the dinoflagellate *Gonyaulax* are correlated with extensive plastid remodeling. One marker for this remodeling is mobilization of ribulose bisphosphate carboxylase/oxygenase (Rubisco) from the plastid periphery to plastid regions nearer the cell center called pyrenoids. Nuclear-encoded proteins such as Rubisco transit through the Golgi in dinoflagellates; hence, we blocked protein import into the plastids using Brefeldin A (BFA) to explore the mechanism for plastid remodeling. We find that pyrenoid formation normally occurs concurrently with increased Rubisco synthesis rates *in vivo*, and when BFA is given prior to the onset of Rubisco synthesis, pyrenoid formation is partially or completely inhibited by 0.1 or 0.3 μg/mL BFA, respectively. Rubisco synthesis itself is not affected, and BFA-treated cells accumulate Rubisco in novel structures we term BFA bodies. Interestingly, when given just after the onset of Rubisco synthesis, BFA delays but does not block Rubisco mobilization, suggesting that a timing signal for plastid remodeling is delivered to the organelles at the same time as newly synthesized Rubisco. BFA also inhibits the circadian increases in carbon fixation rates, supporting the hypothesis that the biochemical basis for this circadian rhythm may be Rubisco distribution within the plastid.

Key words: Brefeldin A, carbon fixation, circadian rhythm, dinoflagellate, protein targeting

Received 14 December 2004, revised and accepted for publication 4 April 2005, published on-line 20 May 2005

Dinoflagellates are eukaryotic protists most closely related to the group of intracellular parasites known as apicomplexans, a relationship supported by both nuclear (1) and plastid (2) gene phylogenies. However, unlike the apicomplexan plastids that are thought to play a role in fatty acid biosynthesis (3) and isoprene formation (4), the dinoflagellate plastids are active in both carbon fixation and oxygen evolution (5). Furthermore, dinoflagellate plastids are surrounded by three membranes instead of four, and this has led to development of an unusual targeting mechanism for nuclear-encoded plastid-directed proteins that involves transit through the Golgi (6). This targeting pathway is used both for stromal proteins, such as carbon-fixing enzyme ribulose bisphosphate carboxylase/oxygenase (Rubisco), and for thylakoid proteins, such as light-harvesting peridinin-chlorophyll (PCP), *a*-binding protein (7).

Dinoflagellates have been studied for over 50 years as a model system for understanding the biochemical basis underlying circadian rhythms. Indeed, many processes with defined rate-limiting steps (RLSs) are clock controlled; hence, the regulatory links between the clock and the observed physiological rhythms can be examined in detail. One such example is the circadian rhythm in photosynthetic carbon fixation, whose RLS is catalyzed by Rubisco. Although there is little daily variation in the amount of immunoreactive Rubisco (5) or enzyme activity *in vitro* (8), there are major circadian changes in the suborganellar localization of Rubisco that occur concurrently with changes in carbon fixation rates (5). In particular, at times of peak carbon fixation rates, Rubisco is found primarily in specialized regions of the plastid termed pyrenoids (9–11). Pyrenoids in dinoflagellates are characterized ultrastucturally by their widely spaced thylakoid stacks and are located near the cell center immediately adjacent to the Golgi. Rubisco constitutes the only known molecular correlate to this extensive plastid remodeling (10,12). Interestingly, as the thylakoid stacks that contain the light-harvesting proteins spread apart, the effective concentration of the oxygen-generating machinery in this region decreases (5). This suggests that sequestration of Rubisco in pyrenoids may result in formation of discrete regions within the organelle, one specialized for carbon fixation and one for oxygen evolution. This in turn may impact on carbon fixation rates, as O_2 is a competitive inhibitor of CO_2 binding to the active site of Rubisco, and the unusual form II Rubisco in dinoflagellates (13) is even more oxygen sensitive than the typically found form I enzyme (14).

The mechanisms underlying the circadian formation of pyrenoids within the plastid are still unknown, as are the control steps linking this rhythm to the circadian clock. Indeed, it is not even known whether this process is intrinsic to the plastid or requires timing signals from the nucleus. This latter question is actually quite difficult to address experimentally, as protein synthesis inhibitors on 80S ribosomes shift the phase of the endogenous circadian clock (15) at doses less than those required for complete inhibition of protein synthesis (16). The effects of protein synthesis inhibitors on plastid ultrastructure (10) have thus been ascribed to effects on circadian timing rather than on plastid protein synthesis. However, the

recent observation that plastid-directed nuclear-encoded proteins transit through the Golgi (6) has suggested that the vesicular transport inhibitor Brefeldin A (BFA) might act as a more specific inhibitor of Rubisco entry into plastids. BFA stabilizes binding between the ADP-ribosylation factors (ARFs) that act as coat recruitment factors by Golgi membranes and an approximately 200 amino acid Sec7 domain in the membrane-bound guanine nucleotide exchange factors (GEFs) that accelerate the replacement of GDP with GTP (17). The crystal structure of the ARF1-GDP-Sec7-BFA complex shows that BFA obstructs the conformational changes in ARF1 required for Sec7 to free the GDP molecule (18), thus blocking vesicle formation. There are no reports to date of an effect of BFA on the circadian clock.

The effects of BFA in mammalian cells are rapid, typically within minutes, and are characterized by disassembly of the Golgi complex and redistribution of its contents into the endoplasmic reticulum (ER) (19). However, it must be noted that other Sec7 domain-containing GEFs might be present in other organisms, with potential effects of blocking the activation of monomeric GTPases involved in signal transduction, nuclear protein transport, or cytoskeleton organization (20). In the dinoflagellate *Gonyaulax*, we find that BFA does indeed inhibit Rubisco import into plastids, although at high concentrations we also find suggestive evidence for an effect of BFA on the cytoskeleton. More importantly, we find that BFA both blocks the formation of pyrenoids and inhibits the normal circadian increase in carbon fixation rates. We conclude that timing signals, in the form of nuclear-encoded proteins transported to the plastid from the Golgi, are necessary to initiate the redistribution of Rubisco that leads to circadian pyrenoid formation.

Results

BFA blocks pyrenoid formation

There are no reports of BFA action on dinoflagellates in the literature; hence, as a first step, the toxicity of the drug was determined. We find that the dinoflagellate *Gonyaulax* is quite sensitive to BFA, with an LD_{50} after 24 h of 0.3 μg/mL. BFA concentrations of 0.1 μg/mL were lethal to less than 20% of cells in the population after 24 h, while concentrations of 0.03 μg/mL or lower did not cause cell death after 24 h. The concentrations of 0.1 and 0.3 μg/mL were thus chosen to represent intermediate and high levels of the drug in subsequent experiments. As our experiments examined the results of inhibiting plastid protein import during a 6-h period encompassing the time of pyrenoid formation, it was important to demonstrate that the concentrations chosen were not toxic to the cells during these shorter-time frame treatments. After 6-h exposure to 0.1 μg/mL of BFA, cells remained actively swimming at the surface. After 6-h treatment with 0.3 μg/mL of BFA, none of the cells were swimming at the surface, but roughly a quarter were observed to be swimming slowly at the bottom of the culture flasks. More importantly, all cells recover full surface swimming activity if the 0.3 μg/mL of BFA is washed out after the 6-h treatment. The two concentrations used here are thus non-lethal during the time frame of our experiments. By comparison, the chronic toxic doses of BFA for dinoflagellates appear intermediate between toxic levels observed for mammalian cells ($LD_{50} = 0.01$ μg/mL) (21) and the apicomplexan *Toxoplasma* (1 μg/mL) (22).

We have previously observed that pyrenoids, when formed, contain most of the plastid's Rubisco (5). For example, Rubisco during late day and early night is spread evenly over the plastid surface in cell sections (Figure 1A), while during late night and early day, Rubisco label density in pyrenoids (gold beads per μm^2) is 11 ± 4 times greater than peripheral regions (Figure 1B). The formation of pyrenoids thus requires either a dramatic change in the distribution of pre-existing Rubisco or an extensive Rubisco degradation and reintroduction of newly synthesized protein from the Golgi adjacent to the developing pyrenoid. To distinguish between these possibilities, we measured Rubisco levels in the presence of cycloheximide in order to estimate the rate of degradation when new protein synthesis was blocked (Figure 1C,D). Rubisco degradation still leaves appreciable levels of protein that must be moved from the peripheral regions of the plastid toward the developing pyrenoid.

In cells treated for 6 h with 0.1 μg/mL of BFA, pyrenoids can still be observed, although their total area appears generally smaller than that of pyrenoids in control cells (Figure 1E). Furthermore, considerable Rubisco can be observed outside the pyrenoid regions by immunogold labeling, with a gold particle distribution in pyrenoids less than 3 ± 1 times that in peripheral regions of the plastid. Clearly, this concentration of BFA impairs but does not block Rubisco movement in the plastids. However, in cells treated for 6 h with 0.3 μg/mL of BFA, the effect on plastid ultrastructure is much more pronounced. First, in stark contrast to the elongated plastids seen in both control cells and in cells treated with 0.1 μg/mL of BFA, the chloroplasts appear as shortened, almost circular structures (Figure 1F,G). Each of these fragments is much smaller than normal plastids, suggesting that at these concentrations, BFA may have secondary effects on the actin cytoskeleton to which the plastids are attached (23). Second, the widely spaced thylakoid membrane stacks characteristic of pyrenoids are never observed, even when plastids close to the nucleus are examined (Figure 1F). Lastly, all plastids are all uniformly labeled with the antibody, independent of their position in the cell, indicating that no Rubisco movement within the plastid had occurred. These observations demonstrate a clear effect of BFA on both plastid ultrastructure and Rubisco distribution within the plastid.

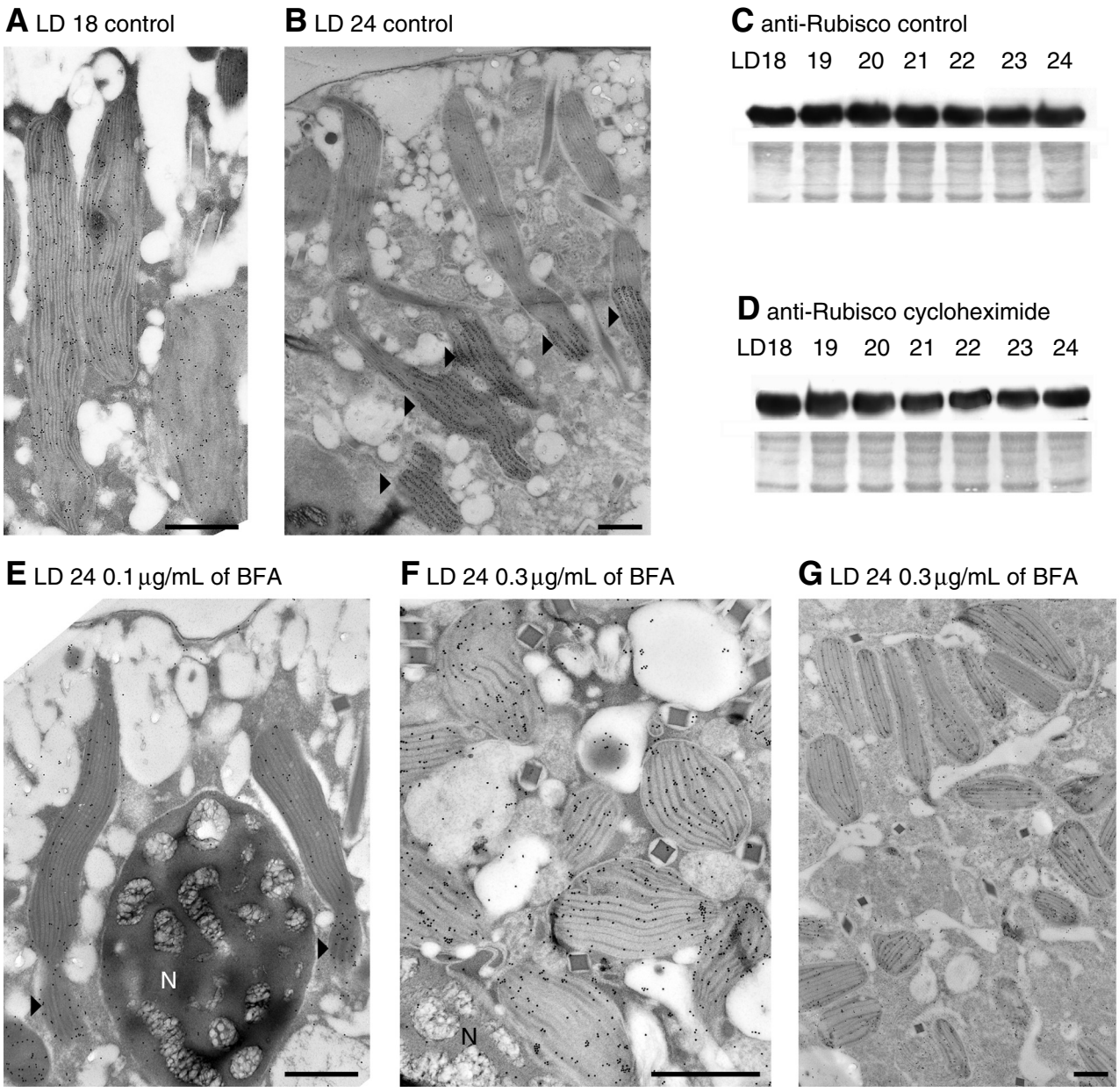

Figure 1: Brefeldin A (BFA) blocks formation of pyrenoids inside the plastids. The ribulose bisphosphate carboxylase/oxygenase (Rubisco) distribution in chloroplasts was observed by anti-Rubisco followed by immunogold labeling. A, B) In control cells at midnight (LD 18), label is spread evenly over the plastid section surface, while at dawn (LD 24), label is seen primarily in pyrenoids (arrows), regions of the plastid with widely spaced thylakoid membranes that are furthest from the cell periphery. C, D) Western blot analysis with anti-Rubisco of cell extracts taken from cultures with or without 100 μM cycloheximide (upper panels). The lower panels show Ponceau-stained membranes as a control for protein load. E) Cells treated with 0.1 μg/mL of BFA contain chloroplasts roughly similar in shape and size to those in control cells, except that less anti-Rubisco staining is concentrated in regions corresponding to the pyrenoid (arrows). Pyrenoids usually form near the nucleus (N). F, G) Chloroplasts in cells treated with 0.3 μg/mL of BFA have lost their typical elongated morphology, and none of the smaller plastids have the expanded thylakoid membranes characteristic of pyrenoids. Scale bars are 1 μm.

BFA treatment blocks Rubisco entry into the plastids

We have previously observed that Rubisco import into *Gonyaulax* plastids involves transit through the Golgi (6). This suggested that the inhibition of pyrenoid formation by BFA might involve a block in the vesicular transport system carrying newly synthesized Rubisco from the Golgi to the plastid. To test this, we first examined the cells for evidence of impaired Rubisco transport in BFA-treated cells. Interestingly, we have never observed Golgi in these cells. Instead, cells treated with 0.3 μg/mL of BFA were found to contain an unusual inclusion body, termed as BFA body, which was never observed in untreated cells

(Figure 2A). This roughly spherical structure is located in the central region of the cell close to the nucleus, the location of the Golgi apparatus in untreated cells (9). The BFA body contains electron-dense and electron-lucent regions, consistent with the presence of both proteins and lipids. At an ultrastructural level, it appears similar to the BFA bodies described in pancreatic β-cells (24).

The addition of BFA to the cell cultures was not expected to inhibit protein synthesis but rather the transport of newly synthesized proteins from Golgi to the plastid. If the BFA body was indeed derived from the Golgi, we reasoned that it should contain newly synthesized nuclear-encoded plastid-directed proteins. Immunoelectron microscopy using the anti-Rubisco clearly showed numerous colloidal gold particles decorating the electron-dense region of the BFA bodies (Figure 2B,C). Labeling was never observed over the electron-lucent regions, consistent with higher protein content in the electron-dense regions.

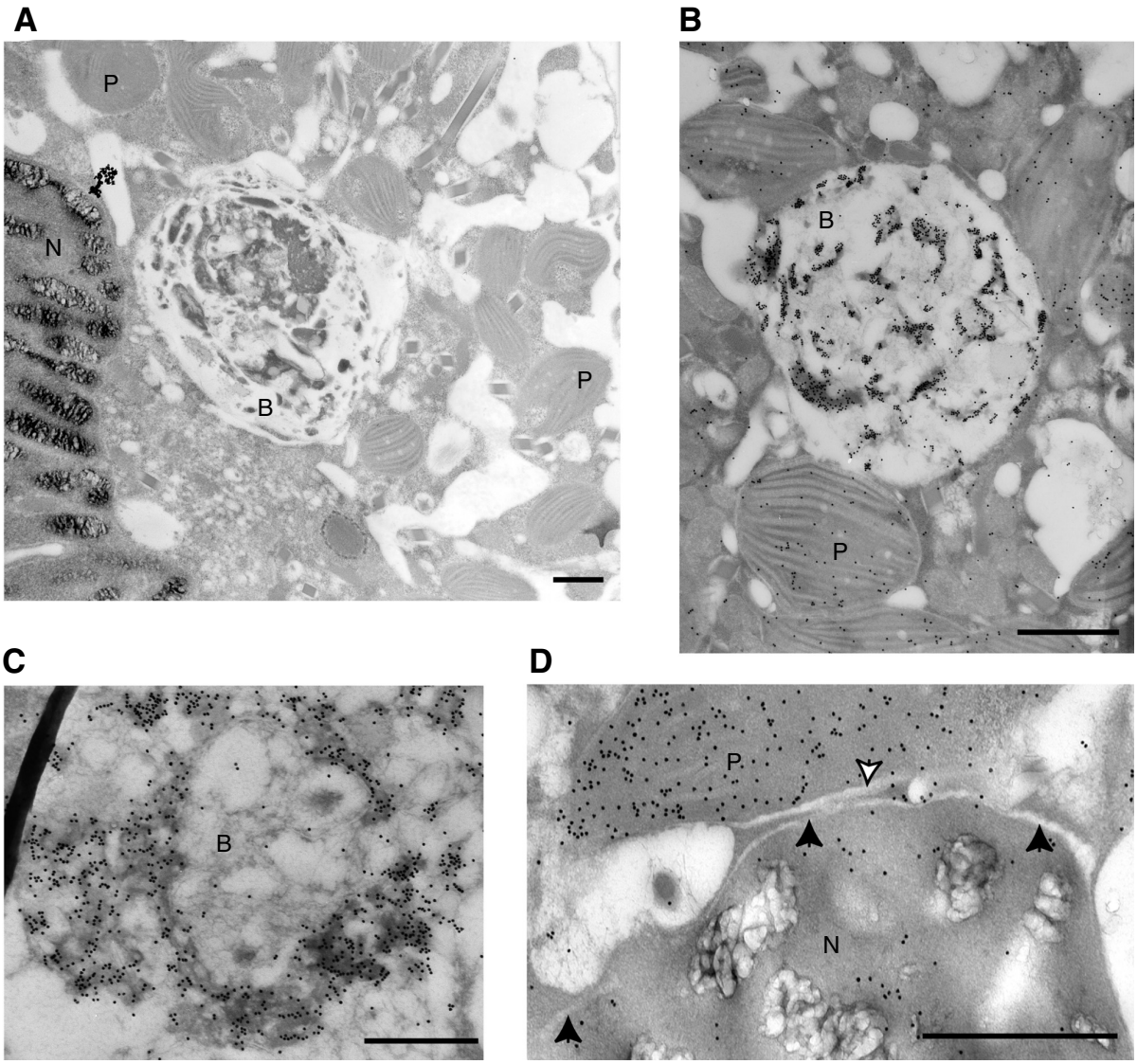

Figure 2: Brefeldin A (BFA) bodies contain membrane and nuclear-encoded plastid-directed proteins. A) Cells at LD 24 treated with 0.3 μg/mL of BFA for 6 h show a novel polyvesicular structure termed a BFA body (B) in the central region of the cell between the nucleus (N) and the plastids (P), a region corresponding to the normal location of the Golgi apparatus. B, C) Staining of cell sections with anti-ribulose bisphosphate carboxylase/oxygenase (Rubisco) and immunogold indicates that Rubisco is associated with the electron-dense regions of the BFA body, which show a label density much greater than that in the surrounding plastids. D) Anti-Rubisco staining has not accumulated in the nuclear envelope (closed arrow) or in the membrane surrounding the plastid (open arrow). Scale bars are 1 μm.

BFA in animal cells inhibits Golgi-derived vesicular transport, including inhibition of the retrieval mechanism normally used to return ER proteins that have escaped to the Golgi. If the site of BFA action was similar in dinoflagellates, plastid proteins would not accumulate in the ER membranes, including those forming the nuclear envelope if this compartment was contiguous with the ER. Indeed, no label was observed over the nuclear envelope (Figure 2D, solid arrow). These results suggest that the BFA body may represent a swollen and aggregated Golgi apparatus that has fused because of an inability to properly return the appropriate components of the vesicular fusion machinery to the ER.

To confirm that the BFA body was accumulating newly synthesized plastid-directed proteins, we decided to quantitate the label density (gold beads/μm^2) after anti-Rubisco labeling in the BFA compartment and in the plastid (Figure 2B) using different BFA concentrations and treatment durations. When 0.3 μg/mL of BFA was given for 6 h and the cells examined at LD 24, we found that the overall average of label density in the BFA compartment was roughly 2.5 fold greater than that found in the plastid in two independent experiments (Table 1). Despite the fact that the BFA body has considerably less volume than the plastids, clearly this structure contains a substantial amount of plastid-directed protein. The proportion of total cellular Rubisco in the BFA body can be estimated by simply multiplying its relative volume (4% that of the plastid) with its label density (2.5 fold that of the plastids) (Table 1). This estimate suggests that up to 10% of the total cellular Rubisco may be found in the BFA body after a 6-h treatment with 0.3 μg/mL of BFA. By comparison, the roughly 5-day doubling time of the cells (25) would require new Rubisco synthesis corresponding to roughly 20% of the total cellular Rubisco each day.

The different effect of lower BFA concentrations on plastid morphology (Figure 1) suggested that retargeting of newly synthesized Rubisco to the BFA body might also be reduced at a lower concentration. To test this, we measured the relative label in the BFA body and in plastids after a 6-h treatment with 0.1 μg/mL of BFA. We found that the label density in the BFA body was now only 0.8 ± 0.3 fold that in the plastid (Table 2), clearly less than the ratio in the BFA body after a 6-h treatment with 0.3 μg/mL of BFA. We interpret this to mean that the diversion of label to the BFA body is incomplete using 0.1 μg/mL of BFA. This suggests that the small pyrenoids formed (Figure 1) may be due to low levels of Rubisco entering the plastid at this drug dose. Indeed, the pyrenoids are not only smaller but contain significantly lower label densities (2.7 ± 0.6, Table 2) than the 11-fold higher levels found in pyrenoids of untreated cells.

As a variation on this experiment, label densities in the BFA body and the plastid were also measured after a 2-h treatment with 0.3 μg/mL of BFA. This concentration was expected to completely block protein import, and we anticipated that treatment for one-third the time should result in one-third the label. In agreement with this, we found that the label density in the BFA body was now roughly equal to that observed over the total plastid surface and that Rubisco concentration in the pyrenoid was only twofold to threefold that in the periphery (Table 2). Here, we attribute the smaller amount of Rubisco diverted toward the BFA body to the shorter time frame during which newly synthesized Rubisco was misdirected rather than to incomplete inhibition as for the low BFA dose above. Taken together, we conclude from these data that Rubisco accumulation in the BFA body results from a block in newly synthesized protein traffic from the Golgi to the plastid.

We also tested for a block in plastid protein import by measuring the amount of ^{35}S-methionine incorporated into the 55-kDa Rubisco large subunit in the presence or absence of BFA. Rubisco is synthesized as a polyprotein in dinoflagellates and must be proteolytically cleaved to the mature 55-kDa large subunit from an approximately 200-kDa precursor (26,27). This processing is likely to occur in the dinoflagellate plastid as has been found for *Euglena* (28): *Euglena* also contains polyproteins, its plastids are also bounded by three membranes, and its plastid protein import pathway is similar (6). In order to resolve the Rubisco from other proteins, crude extracts of radiolabeled proteins were subjected to two-dimensional gel

Table 1: The BFA body after 6-h treatment contains roughly 10% of the total cellular Rubisco[a]

	Volume (μm^3)	Labeling (Experiment 1) (gold beads/μm^2)	Labeling (Experiment 2) (gold beads/μm^2)
Plastids[b]	400[c]	60 ± 5	30 ± 5
BFA body	15[d]	175 ± 45	75 ± 17
BFA/plastid ratio	4%	2.9	2.5

BFA, Brefeldin A; Rubisco, ribulose bisphosphate carboxylase/oxygenase.
[a]Cells were examined at LD 24. The fraction of total cellular Rubisco in the BFA body is calculated from the product of its volume relative to the plastid and its label density relative to the plastid.
[b]Plastids contain no pyrenoids after a 6-h treatment with 0.3 μg/mL of BFA
[c]Total cellular plastid volume was calculated from the number of organelles in untreated cells (approximately 60 per cell) and the volume of one plastid (calculated as a 8-μm cylinder with 1-μm diameter).
[d]Volume of the BFA body was calculated as a sphere of diameter 3 μm.

Table 2: BFA body labeling and Rubisco enrichment in pyrenoids at LD 24

	6-h treatment with 0.1 μg/mL of BFA (gold beads/μm^2)	2-h treatment with 0.3 μg/mL of BFA (gold beads/μm^2)
Total plastid surface	22 ± 6	32 ± 10
BFA body	17 ± 2	29 ± 3
BFA body/plastid	0.8 ± 0.3	0.9 ± 0.4
Plastid pyrenoid	49 ± 5	60 ± 19
Plastid periphery	18 ± 2	27 ± 9
Pyrenoid/periphery	2.7 ± 0.6	2.2 ± 1.5

BFA, Brefeldin A; Rubisco, ribulose bisphosphate carboxylase/oxygenase.

electrophoresis. Western blot analysis confirmed the identity of a group of three major protein isoforms at 55 kDa as Rubisco (Figure 3A). In untreated cells, incorporation of radiolabel into the 55-kDa Rubisco could be observed in samples labeled between LD 20 and LD 24 (Figure 3B). However, no radiolabel was detected in the mature Rubisco subunits at LD 24 after a 6-h treatment with 0.3 μg/mL of BFA (Figure 3B). Although we were unable to detect the approximately 200-kDa precursor on Western blots after BFA treatment, a problem we attribute to formation of highly insoluble Rubisco aggregates within the BFA bodies, our experiments in the ensemble show that BFA does indeed inhibit protein import to the plastid from the Golgi.

A timing marker for initiating pyrenoid formation enters plastids concurrently with Rubisco

To further probe the relationship between new protein synthesis and pyrenoid formation, plastid ultrastructure was examined in cells treated with BFA at LD 22, 2 h following the onset of Rubisco synthesis. We reasoned that if entry of a newly synthesized protein served as a timing marker for the initiation of pyrenoid formation then these structures should still form when protein import was blocked. Alternatively, if pyrenoids required sustained protein synthesis for their maintenance then the pyrenoids should collapse following a block in protein import. When cells treated at LD 22 with 0.3 μg/mL of BFA were observed at LD 24, pyrenoids had formed as judged by the increased spacing between thylakoid membranes (Figure 4A,C). However, recruitment of Rubisco to the region of the pyrenoid is incomplete, as peripheral regions of the plastids still contain substantial levels of Rubisco (Figure 4B). Counts of the label density in the pyrenoid show that the enrichment is less than threefold that in peripheral regions of the plastid after this 2-hour BFA treatment (Table 2). Rubisco import to the plastid has been interrupted, as confirmed by the presence of BFA bodies that contain substantial levels of anti-Rubisco label (Figures 4C,D). Interestingly, these results indicate that the formation of a morphologically distinct pyrenoid is not a direct result of accumulating the entire organelle's Rubisco in this area, and that thylakoid spacing increases and Rubisco accumulation may be independent processes.

It was also possible that these low–Rubisco-content pyrenoids might represent intermediates in a process of pyrenoid breakdown rather than a slower rate of pyrenoid formation. We thus also examined cells treated with BFA at LD 22 at LD 2. In these samples, pyrenoids can be clearly seen (Figure 4E) and contain Rubisco enriched by a factor of roughly 10-fold as determined by anti-Rubisco staining (Figure 4F). As the level of Rubisco recruitment has proceeded to the same extent as for control cells observed at LD 24, we conclude that pyrenoid formation was merely delayed by the LD 22 BFA treatment. We interpret these results to indicate that pyrenoid formation is initiated by a timing signal imported into the plastid from the Golgi between LD 18 and LD 22. This signal initiates pyrenoid formation immediately and appears to act catalytically in Rubisco recruitment, as blockage of vesicular transport after LD 22 retards but does not block pyrenoid formation. Finally, we also conclude that continued Rubisco synthesis is not necessary for maintenance of the pyrenoids or the asymmetric Rubisco distribution within the plastid.

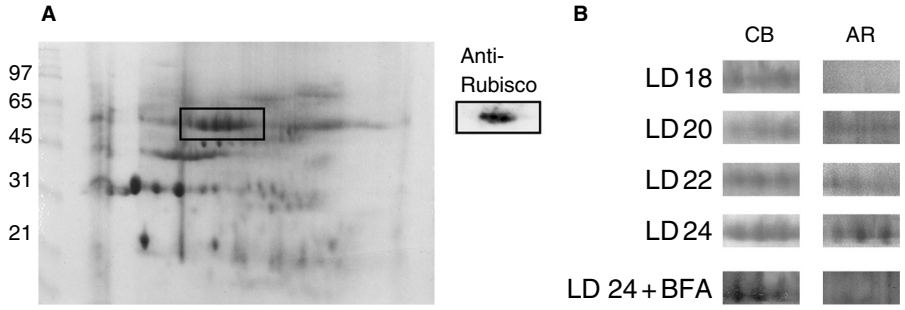

Figure 3: Brefeldin A (BFA) blocks import of nuclear-encoded plastid-directed proteins. A) Ribulose bisphosphate carboxylase/oxygenase (Rubisco) can be resolved from other protein components in the cells by two-dimensional gels. The identity of the protein isoforms in the boxed area as Rubisco can be confirmed by anti-Rubisco staining on Western blots. B) *In vivo* metabolic labeling with ^{35}S-methionine shows that amount of signal after autoradiography (AR) in the position associated with the Rubisco as determined by Coomassie blue staining (CB) depends on the time of labeling. No label is associated with the 55-kDa Rubisco isoforms at LD 18 in untreated cells or at LD 24 in cells treated for 6 h with 0.3 μg/mL of BFA. Other proteins are synthesized normally after BFA treatment, although only the position corresponding to Rubisco is shown here.

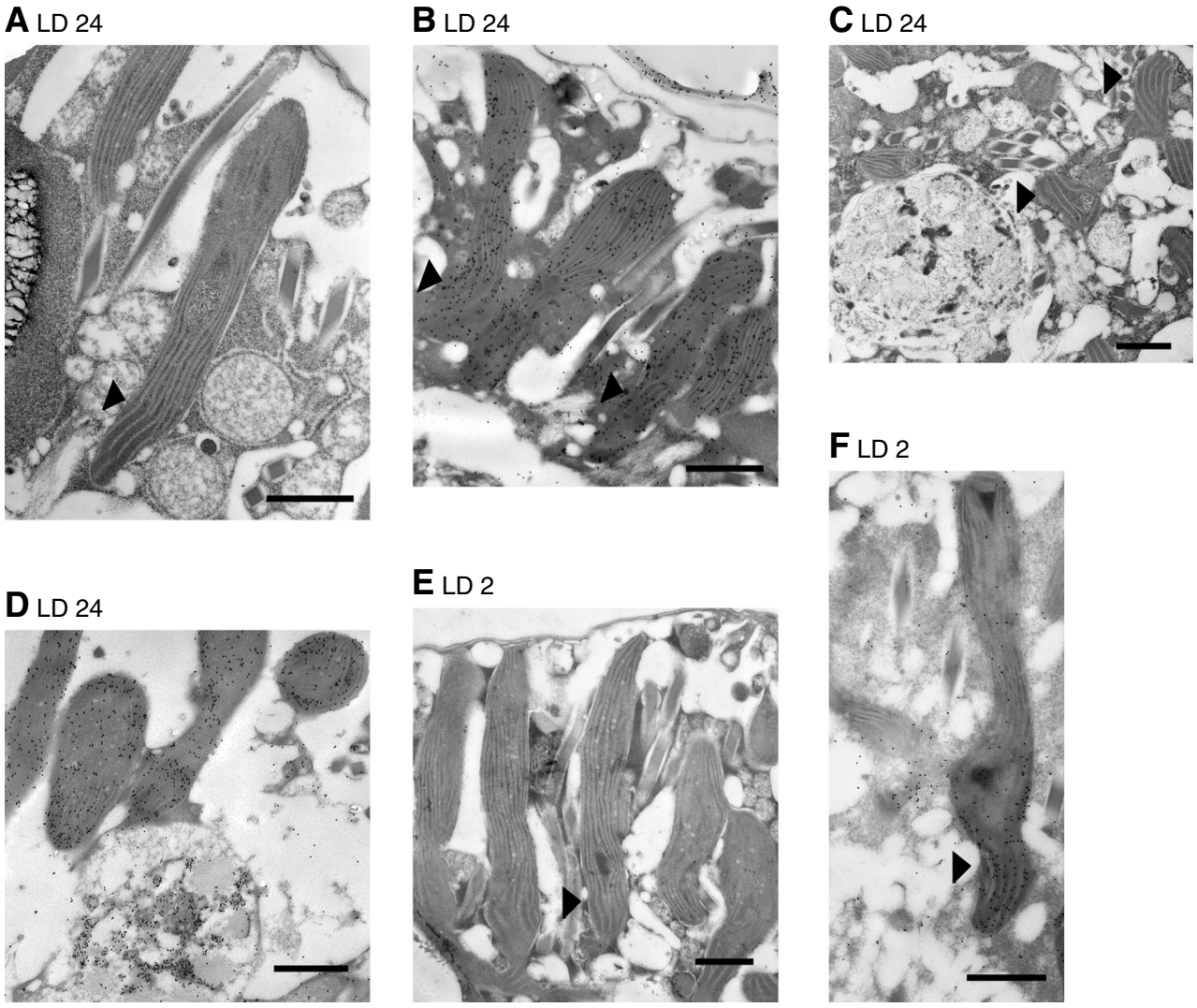

Figure 4: Addition of Brefeldin A (BFA) after the onset of ribulose bisphosphate carboxylase/oxygenase (Rubisco) synthesis delays Rubisco accumulation but does not stop pyrenoid formation. A–D) In cells at LD 24, after a 2-h exposure to 0.3 μg/mL of BFA, pyrenoids (arrows) can be observed in plastids that have maintained their normal elongated morphology. The distribution of Rubisco, determined by anti-Rubisco and immunogold staining, shows that considerable marker is found in peripheral regions of the plastid. BFA bodies form after 2 h of BFA treatment, indicating that the drug has had the expected effect on vesicular transport and that the BFA bodies contain Rubisco as shown by immunogold labeling. E, F) In cells at LD 2, after a 4-h exposure to 0.3 μg/mL of BFA, pyrenoids are formed and plastid morphology is normal. The gold particle distribution inside the plastids, determined after anti-Rubisco staining, indicates that Rubisco accumulation in the pyrenoid is complete. Scale bars are 1 μm.

BFA does not block pyrenoid breakdown

The preceding results suggested that pyrenoid formation might be regulated by import of newly synthesized proteins into the plastids. However, the disappearance of the pyrenoids is also a circadian-controlled process. To determine whether a specific signal imported from the Golgi was implicated in pyrenoid breakdown, BFA was administered to the cells at LD 12, 2 h before pyrenoids have disappeared (Figure 5A). We observe the same plastid morphology at LD 14 in both treated and untreated cells (Figure 5B,C). In both samples, the plastids have pulled back from the cell wall and no pyrenoids are present. This indicates that inhibition of vesicular traffic is unable to retard chloroplast movement in the cell and the decrease in thylakoid spacing and suggests that any timing signals required for pyrenoid breakdown may impact the plastid using other mechanisms. Although formally possible that pyrenoid breakdown may be due to lack of new protein import at this time in the LD cycle, this seems unlikely given that the pyrenoid do not disappear when new protein import is blocked at LD 22.

BFA blocks increases in CO_2 fixation rates

To determine if BFA-induced changes in plastid ultrastructure would also have an impact on chloroplast function, we

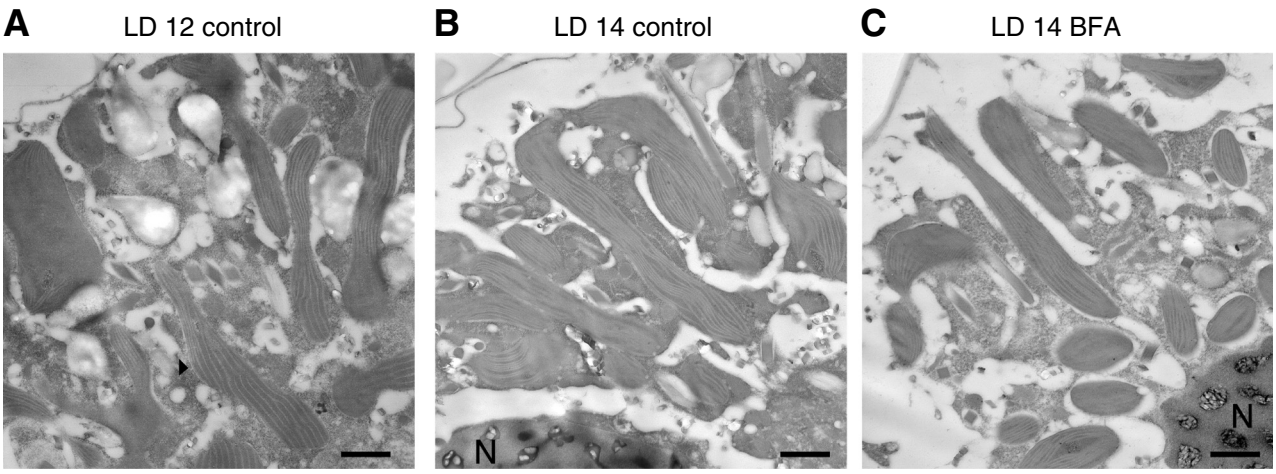

Figure 5: Brefeldin A (BFA) does not inhibit pyrenoid breakdown. A, B) In control cells, pyrenoids are still present in plastids at LD 12 but have disappeared by LD 14. C) The disappearance of pyrenoids is not inhibited by a 2-h treatment with 0.3 μg/mL of BFA. Scale bars are 1 μm.

measured carbon fixation rates *in vivo* using incorporation of $H^{14}CO_3^-$ (Figure 6). As previously shown for samples in constant light (5), carbon fixation rates in control cultures under LD cycles also increase threefold to fourfold from a minimum at midnight (LD 18 on a LD 12:12 cycle) to a maximum roughly 6 h later (LD 24). In contrast, carbon fixation rates in cultures treated with either 0.1 or 0.3 μg/mL of BFA did not increase to the same extent. In samples treated with 0.1 μg/mL of BFA, carbon fixation rates increased roughly in parallel with control cultures for 2 h, but after 6-h total treatment with the drug, the carbon fixation rates were roughly double the values at LD 18. The effect in cells treated with 0.3 μg/mL of BFA was even more pronounced, with carbon fixation rates after 6-h treatment almost the same as that found at LD 18. These results indicate that the normal circadian increases in carbon fixation rates in *Gonyaulax* are also sensitive to BFA.

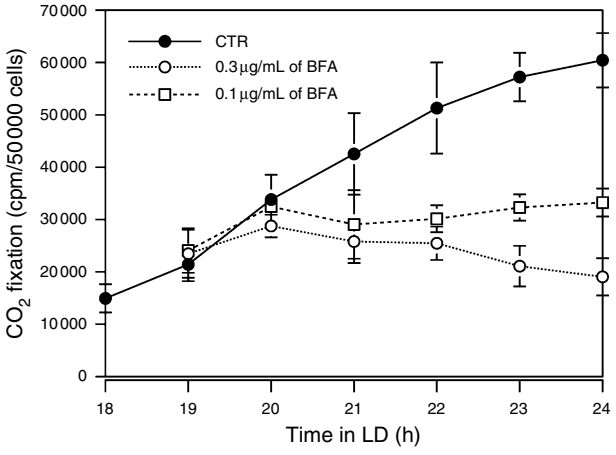

Figure 6: Brefeldin A (BFA) blocks the normal nightly increase in CO_2 fixation. In the absence of BFA, rates of ^{14}C-CO_2 fixation in *Gonyaulax* cultures increase from midnight (LD 18) to dawn (LD 24). This normal nightly increase can be blocked by addition of either 0.1 or 0.3 μg/mL of BFA to cell cultures at LD 18.

BFA does not affect pyrenoid formation by altering clock timing

The results showing that the timing of BFA application is important for inhibition of pyrenoid formation suggested the possibility that the effects of the drug could be an indirect result of an effect on the circadian clock. To test this, two other circadian rhythms were monitored following application of the drug. In one, the timing of the bioluminescence glow peak was measured (Figure 7A). The reduced peak level in luminescence after BFA addition is due to stimulation of light emission by BFA, although the timing of this circadian rhythm is clearly unaffected by BFA. In another, the timing of cell division was monitored. In control cells, mitosis is gated to LD 1, as seen by the characteristic paired cells when the cell cultures are examined microscopically. In BFA-treated cells, the timing of entry into M-phase was not altered, as paired cells were first observed at LD 1, and the percentage of cell pairs is similar between treated and untreated. However, the BFA-treated cells were not able to complete mitosis, as paired cells were also observed at LD 2 and LD 3. In contrast, control cells at these latter times never have paired cells, and instead many small recently divided cells can be observed. We interpret this latter result as indicative of the requirement for vesicular transport during the formation of new cell walls analogous to the BFA-induced disruption of the terminal phase of cytokinesis in the embryonic blastomeres of BFA-treated *Caenorhabditis elegans* embryos (29). Taken together, these experiments indicate that BFA exerts its effect on pyrenoid formation and carbon fixation directly rather than by an indirect effect on the phase of the circadian oscillator during the time frame of our experiments. Furthermore, these experiments also show that the normal cellular metabolism

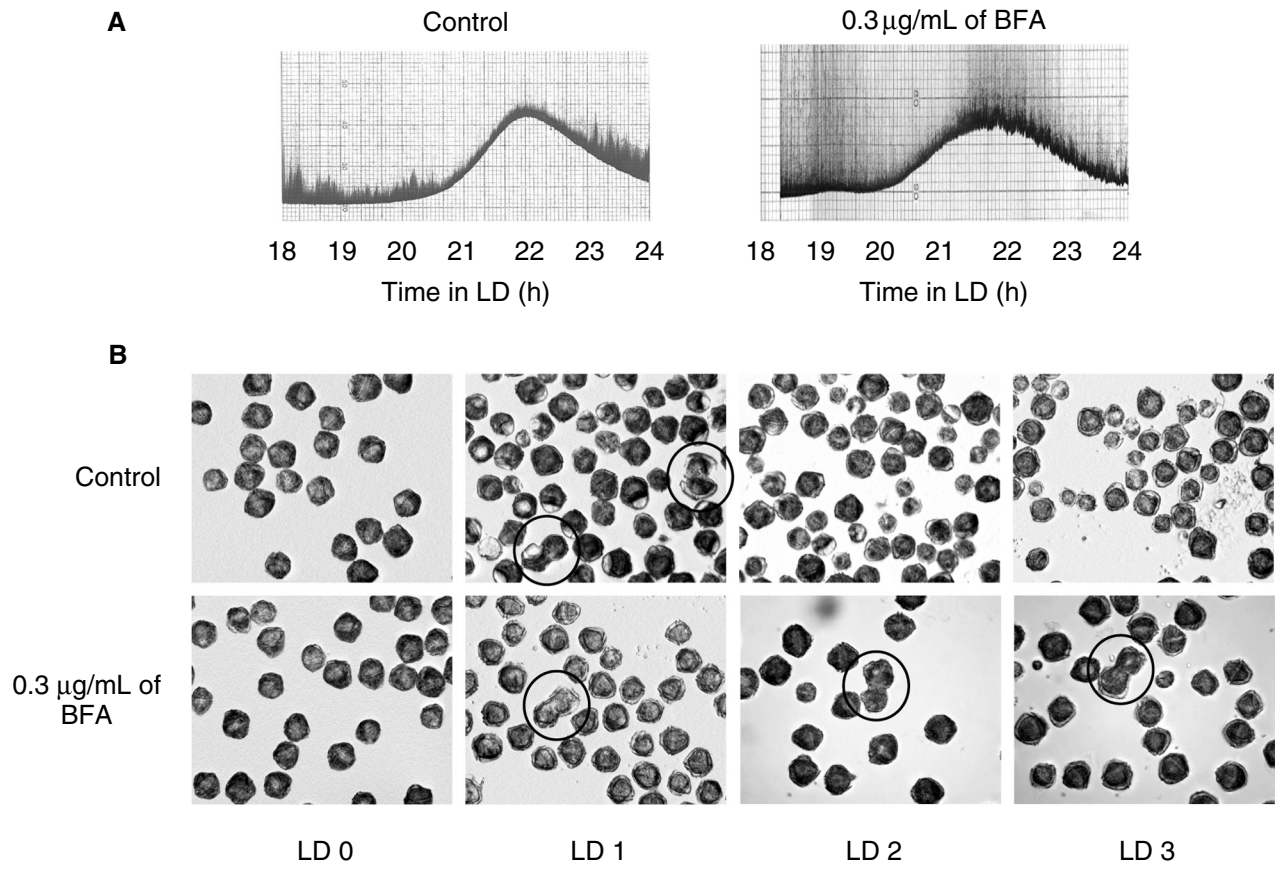

Figure 7: Brefeldin A (BFA) does not affect the timing of cell division or bioluminescence rhythms. A) Chart paper trace recordings of cells placed adjacent to a photomultiplier tube show luminescence emission as both flashes (vertical spikes) and glow (base line). The peak in bioluminescence glow occurs at roughly LD 22 in both control cell cultures and those to which 0.3 μg/mL of BFA was added at LD 18. The experimental curve begins at LD 18.5 as BFA addition results in considerable luminescence. Note that the scale used for the BFA-treated sample has been expanded to more clearly identify the peak time. B) Mitosis can be observed microscopically by the presence of characteristic paired cells (circles). Normally gated by the circadian clock to 1 h after dawn (LD 1), paired cells can be seen at this time both in control cultures and cultures to which 0.3 μg/mL of BFA was added at LD 18. However, treated cultures contain also paired cells at later times and lack the many smaller cells indicating completion of mitosis.

underlying these events has proceeded normally, supporting the lack of BFA toxicity during these 6-h experiments.

Discussion

Circadian rhythms represent the observed outputs of circadian timers commonly found in eukaryotic cells. Studies using DNA microarray technology have contributed greatly to our understanding of observed rhythms by documenting the numerous changes in gene expression that can be directly regulated by the circadian oscillator (30). These studies, however, imply that changes in gene expression will regulate the activity of biochemical pathways by altering the amounts of enzymes catalyzing the RLS in the pathway. In this context, regulation of the circadian rhythm of carbon fixation in the dinoflagellate *Gonyaulax* is somewhat unusual. Instead of changes in enzyme amounts, the circadian rhythm in carbon fixation rates correlates with circadian changes in the suborganellar distribution of the RLS catalyst Rubisco. This conclusion is based on the observations that the amount of Rubisco remains relatively constant over the daily cycle, while the Rubisco concentration in pyrenoids increases 10-fold concurrently with the increase in carbon fixation rates (5).

The experiments described here support the view that the carbon-fixing activity of Rubisco is intricately linked to the distribution of the enzyme within the plastid, as BFA treatment blocks both Rubisco recruitment to the pyrenoids (Figure 1) and the normal circadian increase in carbon fixation rates (Figure 6). The molecular mechanism whereby changes in Rubisco distribution affect CO_2 fixation rates is not yet known, although it is possible that the changes in Rubisco distribution alter the relative levels of the substrate CO_2 and the competitive inhibitor O_2. The concentrations of substrate and inhibitor affect the $\upsilon CO_2/\upsilon O_2$ ratio that ultimately determines the activity of the enzyme (31). Interestingly, the thylakoid membranes

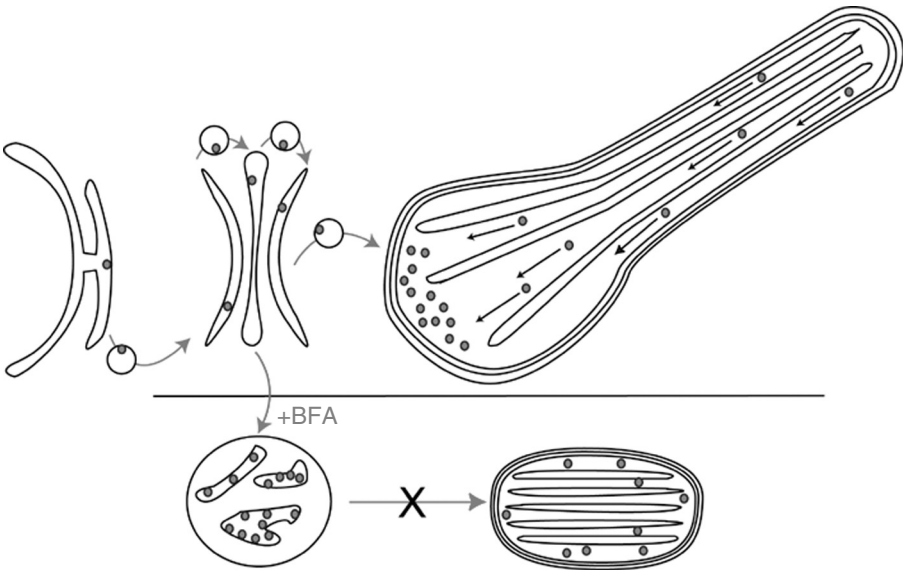

Figure 8: Schematic model of Brefeldin A (BFA) inhibition of ribulose bisphosphate carboxylase/oxygenase (Rubisco) import into plastids. Rubisco is normally synthesized on membrane-bound ribosomes and transported to the Golgi where it is targeted to the chloroplasts. The import of newly synthesized protein correlates with development of the pyrenoid and movement of Rubisco from the peripheral regions of the plastid to regions close to the Golgi. BFA treatment blocks Golgi to plastid transport, and when BFA is given before the onset of Rubisco synthesis, completely inhibits pyrenoid formation and Rubisco movement. Plastid-directed protein accumulation in BFA bodies is proportional to the amount of protein synthesized.

contain the major light-harvesting protein PCP (7), so that as Rubisco accumulates in the pyrenoid and the spacing between the thylakoid membranes increases, the relative amount of PCP in the pyrenoid decreases. Our calculations show that the pyrenoid contains roughly 90% of the plastid Rubisco yet less than 20% of the plastid PCP (5). Thus, Rubisco recruitment to the pyrenoid has the added benefit of reducing the impact of the O_2-generating machinery. Taken together, these data support the contention that Rubisco can fix carbon more efficiently when sequestered into pyrenoids.

While circadian changes in Rubisco synthesis rates do not appreciably change the cellular levels of the enzyme, new protein synthesis does appear to be required for recruitment of Rubisco to the pyrenoids. Our schematic model for this (Figure 8) is supported by the observation that pyrenoid formation is inhibited when BFA blocks newly synthesized Rubisco from entering the plastids (Figure 1). To confirm that Rubisco entry into the plastids was in fact blocked by BFA, we first evaluated the label density following anti-Rubisco staining in the BFA bodies relative to that in the plastids after exposure of the cells to BFA. To be a good indicator of inhibition of plastid protein import, this measure requires that the inhibition of vesicular transport by BFA in *Gonyaulax* is as rapid as has been found in mammalian cells (19). In support of this, we observe well-formed BFA bodies that stain strongly with the anti-Rubisco after only a 2-h BFA treatment, suggesting that BFA does indeed act quickly in dinoflagellates. To determine whether the BFA body contained all the Rubisco synthesized subsequently to administration of the drug, we first estimated the relative volume of the BFA body and the plastids. We assumed the chloroplasts to be cylinders and the BFA body to be a sphere and estimated from this that the BFA body had a volume of approximately 4% that of the plastids (Table 1). The concentration of Rubisco in the BFA body, however based on the gold particle density after anti-Rubisco labeling, is approximately 2.5 times greater than that in the plastids. This suggests that after a 6-h BFA treatment, the BFA body might contain up to 10% of the total cellular Rubisco. This seems reasonable, given that the generation time of the cells under our growth conditions is roughly 5 days (25) and that Rubisco is only synthesized for roughly 10-h each day (32). A 6-h exposure to 0.3 μg/mL of BFA could indeed stop the equivalent of one-tenth of the total cellular Rubisco from entering the plastid. It is interesting that when the duration of BFA treatment is reduced from 2 to 6 h or when the concentration of BFA is lowered from 0.3 to 0.1 μg/mL, the BFA body now contains a label density roughly equal to that in the plastid (Table 2), suggesting that only approximately 4% of the total cellular Rubisco is now found in the BFA body. These values are all consistent with an inhibition of Golgi to plastid transport by BFA.

The inhibition of protein import into plastids by BFA was also evaluated from the amount of radiolabel incorporated into the mature 55-kDa Rubisco large subunit *in vivo*. This measurement exploits the fact that dinoflagellate 55-kDa Rubisco is normally synthesized as a approximately 200-kDa polyprotein precursor (13,26,27). The cleavage of the polyprotein to yield the mature 55-kDa large subunit is assumed to occur in the dinoflagellate plastid stroma, an assumption supported by the plastid processing shown for polyproteins entering *Euglena* plastids (28), which like those of dinoflagellates are bounded by three membranes and use the same protein-trafficking mechanism (33). This protein-trafficking mechanism is quite unusual, as plastid-

directed proteins synthesized *in vitro* in the presence of canine microsomes are attached to the membranes yet fully susceptible to protease treatments (6,34). This suggests that *in vivo,* the plastid-directed proteins may be transported with the bulk of the protein in the cytoplasm. As the polyproteins have only a single N-terminal targeting and membrane-attachment domain, processing prior to arrival at the plastid would leave considerable Rubisco in the cytoplasm at odds with experimental observations (5). Processing to the mature 55-kDa form is thus likely to be a reliable indicator of plastid import, and as we observe no Rubisco labeling in the presence of BFA, Rubisco import to the plastid must have been impaired. Interestingly, the unusual protein-trafficking mechanism used by dinoflagellates might also contribute to formation of the BFA bodies by aggregating together Golgi and transport vesicles whose transport to the plastid has been blocked. This type of aggregation could make the proteins difficult to extract and might explain why Western blots fail to reveal the presence of the approximately 200-kDa polyprotein precursor. In any event, the lack of radiolabel incorporated into mature Rubisco subunits in BFA-treated samples, while other proteins incorporate radiolabel normally, which argues strongly for inhibition of Golgi to plastid transport by BFA.

Surprisingly, we have observed that when BFA is added after Rubisco synthesis has started, morphologically recognizable pyrenoids containing less Rubisco than normal can be observed (Figure 4). This suggests that pyrenoids are not formed by recruitment of Rubisco into the region of the developing pyrenoid and a consequent separation of the thylakoid stacks as one might suspect. Instead, it appears that pyrenoids form prior to recruitment of Rubisco from the periphery. This observation thus requires one timing signal, for separating the thylakoid stacks (which is completed rapidly after reception of the signal even if protein synthesis is blocked) and another for Rubisco recruitment (which is completed rapidly only if protein synthesis is ongoing). Is one of the signals, which appear to arrive concurrently with Rubisco, Rubisco itself? This cannot be answered definitively at present, as Rubisco is the only protein synthesized at this time for which antibodies are available. Indeed, it is just as likely that the timing signal is an accessory protein, synthesized and imported at the same time as Rubisco. It is important to note that the extent of pyrenoid formation closely parallels the amount of Rubisco entering the plastid. For example, a 6-h treatment with 0.1 μg/mL of BFA or a 2-h treatment with 0.3 μg/mL of BFA has intermediate Rubisco label densities in the BFA body and intermediate enrichments of Rubisco in the pyrenoids (Table 2). Both treatments thus appear to reroute the same amount of Rubisco to the BFA bodies, to the detriment of the developing pyrenoids. Thus, if an accessory protein is involved, its synthesis must closely parallel that of Rubisco. It would be of interest to determine whether RNAi could be used to inhibit Rubisco synthesis, as this would provide the most specific tool to date for determining the role of new Rubisco synthesis itself in the regulation of pyrenoid formation and Rubisco recruitment. However, no studies have yet reported tests of RNAi in dinoflagellates.

It is noteworthy that continued protein import into the plastid is not required for pyrenoid maintenance once they have formed. The inhibition of Rubisco import by BFA treatment at LD 22 does not collapse the pyrenoids (Figure 4), and this underscores the importance of Golgi-derived timing signals as opposed to continued Rubisco synthesis. It is puzzling therefore that BFA was not able to inhibit pyrenoid breakdown at LD 12. It is possible that the regulation of circadian pyrenoid breakdown may utilize a different mechanism. Alternatively, a circadian-timing signal may have passed through to the plastid prior to the time when BFA was administered.

A second unexpected finding was the production of large numbers of smaller, almost spherical plastids from the normal elongated plastid morphology by exposure of cells to 0.3 μg/mL of BFA at LD 18 (Figure 1C,D). This suggests that BFA may have secondary effects at high concentrations and is especially interesting in that this unusual plastid morphology is not observed when BFA is given at LD 22 (Figure 4) or at LD 12 (Figure 5). One possible explanation for this observation is related to the timing of the circadian plastid elongation. Normally, the chloroplasts become more elongated until they extend out to the cell periphery at a time roughly between LD 20 and LD 22 (10). It seems reasonable to assume that if BFA was able to influence changes in plastid morphology that this might occur at the time plastid morphology is normally changing, and that BFA given after the change has already taken place might be ineffective. Interestingly, circadian changes in plastid morphology in the dinoflagellate *Pyrocystis* can be inhibited by cytochalsin D, which depolymerizes the actin cytoskeleton (23). One possible connection between the actin cytoskeleton and BFA lies in the recently described Arfaptin, capable of binding Arf-GTP as well as Rac-GTP or Rac-GDP in mammalian cells (35). A blockage of Arf activation by BFA would thus free Arfaptin for Rac binding, which could then result in alteration of the actin cytoskeletal conformation. It would thus be interesting to examine plastid movement in *Pyrocystis* after BFA addition.

It must be stressed that the inhibition by BFA of the normal increases in circadian carbon fixation rates (Figure 6) has a much more defined effect on the rhythm than that brought about by general protein synthesis inhibitors. The reason for this is that general protein synthesis inhibitors have a major impact on the clock itself. For example, the inhibitors anisomycin (15) or cycloheximide (36) can shift the phase of the circadian clock by 12 h or more. Furthermore, ultrastructural changes in plastid morphology brought about by

cycloheximide pulses all appear to be consistent with changes in clock phase rather than in blocking plastid protein synthesis (10). Lastly, as phase shifting occurs at doses of the protein synthesis inhibitor less than those required to fully block protein synthesis (16), cycloheximide-induced blockage of pyrenoid formation is not likely to be due to an inhibition of plastid protein synthesis. In contrast, we find that BFA treatment has no effect on the timing of either the bioluminescence glow or cell-division rhythms over the course of our experiments (Figure 7). As the phases of photosynthesis, bioluminescence and cell division are tightly coupled under normal growth conditions (37), this indicates that the effects of BFA on the carbon fixation rhythms are not likely to be secondary effects resulting from an impact of the drug on the clock mechanism. Thus, inhibition of the photosynthesis rhythm by BFA must rather be a result of blocked protein import into the plastid.

It is worth at this point to compare the mechanisms used for regulating the carbon fixation and bioluminescence rhythms. The bioluminescence capacity of the cells correlates with increases in the cellular levels of the substrate luciferin (38), the luciferin-binding protein LBP (39) and the reaction catalyst luciferase (40,41). Protein levels are regulated at the level of synthesis (39) using a translational control mechanism (42). Both LBP and luciferase are assembled into discrete organelles termed scintillons during maximum light emission (43). Scintillon formation begins at the time of LBP synthesis, and double immunolabeling experiments show that small prescintillons can be detected as aggregates of both luciferase and LBP in the cytoplasm near the nucleus (44). These small prescintillons aggregate and move out toward the periphery of the cell where they become active as mature scintillons when they come in contact with the vacuolar membrane. The changes in bioluminescence capacity thus reflect changes in protein synthesis rates, protein amount and protein distribution within the cytoplasm. By comparison, we show here that changes in carbon fixation capacity reflect changes in protein synthesis and protein distribution in the chloroplast. In both cases, changes in levels of gene expression (at the translational level) initiate changes in protein localization that ultimately are observed as the rhythm. While the mechanism modulating Rubisco distribution may be subtler, a basic theme of enzyme localization appears conserved in these two rhythms.

Materials and Methods

Cell growth and viability measurements

Cell cultures of *Gonyaulax polyedra* (strain number 1936, Provasoli-Guillard Center for Culture of Marine Phytoplankton, Boothbay Harbor, Maine) were grown under a 12 h light/12 h dark cycle (60 μmol/m^2/second white fluorescent light) at 16 °C in f/2 medium as described (45). During the typical 24-h cycle, the start of the light phase is termed LD 0, while the onset of darkness is called LD 12. For treatment of the cultures with BFA (Sigma, St Louis, MO, USA), a 10 mg/mL of stock solution was made in dimethyl sulfoxide and was further diluted to working solution of 1 mg/mL in dimethyl sulfoxide before use. For each BFA concentration experiment, either BFA or solvent alone was added at different concentrations at middle of the night phase, and samples were taken at hourly intervals for 6 h and after 24 h for determination of the percent viable cells by staining with the vital dye Evan's blue (46).

Metabolic labeling and electrophoresis

For each sample, a 100 mL aliquot of cell culture was removed and concentrated to 1 mL using a 20-μm Nylon filter. The samples were pretreated with 1 μL of 100 μM chloramphenicol in ethanol for 10 min prior to labeling with 200 μCi of ^{35}S-methionine for 20 min in the dark at 16 °C. The cells were then washed three times with fresh f\2 medium to remove excess radiolabel and five times with 0.4 M sucrose to remove the salt. The cell pellet was resuspended in 200 μL of 4% Chaps, and the cells were mechanically disrupted using a mini-beadbeater (Biospec Products, Bartlesville, OK, USA). The extract was clarified by centrifugation at 14 000 × *g* for 10 min at 4 °C, and the protein was precipitated from the supernatant by addition of 1 mL of acetone at −20 °C. The protein pellet recovered by centrifugation was washed 10 times with cold 70% acetone before resuspension in UTC buffer (7 M Urea, 2 M thiourea, 4% Chaps, 0.02 M DTT, 0.5% pH 4–7 IPG buffer (Amersham Biosciences, Baie d'Urfé, Quebec, Canada). The samples were centrifuged at 14 000 × *g* for 15 min, and the supernatant was allowed to rehydrate a pH 4–7 IEF strip (Amersham-Pharmacia Biotech) overnight at 20 °C. The samples were focused at 500 V for 1 h, 1000 V for 1 h and 8000 V for 6 h. The strips were then equilibrated for 15 min in 10 mL of equilibration buffer (50 mM Tris-HCl pH 8.8, 6 M urea, 30% glycerol, 2% SDS, 0.005% Bromophenol blue, 10 mg/mL DTT), and a 15-min incubation in 10 mL of equilibration buffer containing 25 mg/mL of iodoacetamide. The strips were then electrophoresed on a standard SDS-polyacrylamide gel as a second dimension. The gels were stained with Coomassie Blue, dried using a gel drier and exposed to film at −80 °C for 7 days.

Western blot analyses with anti-Rubisco, either with or without addition of 100 μM cycloheximide, were performed as described (5).

Immunoelectron microscopy

Cells were harvested and washed with 0.4 M phosphate buffer and fixed with 3% glutaraldehyde in 0.4 M phosphate buffer for 30 min, washed three times in PBS and water, followed by standard dehydration procedures and embedded in LR White resin as recommended by the manufacturer. Immunostaining and electron microscopy were preformed as previously described (5).

Carbon fixation measurements

CO_2 fixation rates were measured from conversion of $NaH^{14}CO_3$ to acid-insoluble material. For each assay, 1 μCi radiolabeled bicarbonate was added to each of five 10-mL aliquots of cell culture. The cultures were preincubated under saturating white light (300 μmol/m^2/second) for 3 min, the carbonate was added, and the exposure to bright light continued for a further 15 min, over which time radiolabel incorporation is linear. The cells were recovered on GF/A filters, washed twice with 10 mL of f/2 medium and exposed to HCl vapor overnight. Radioactivity was measured in a LKB scintillation counter after addition of scintillation cocktail.

Acknowledgments

We thank Louise Pelletier for assistance with sample preparation for electron microscopy. We gratefully acknowledge the financial support of the National Science and Engineering Research Council of Canada.

References

1. Van de Peer Y, Baldauf SL, Doolittle WF, Meyer A. An updated and comprehensive rRNA phylogeny of (crown) eukaryotes based on rate-calibrated evolutionary distances. J Mol Evol 2000;51:565–576.
2. Zhang Z, Green BR, Cavalier-Smith T. Phylogeny of ultra-rapidly evolving dinoflagellate chloroplast genes: a possible common origin for sporozoan and dinoflagellate plastids. J Mol Evol 2000;51:26–40.
3. Waller RF, Keeling PJ, Donald RG, Striepen B, Handman E, Lang-Unnasch N, Cowman AF, Besra GS, Roos DS, McFadden GI. Nuclear-encoded proteins target to the plastid in Toxoplasma gondii and Plasmodium falciparum. Proc Natl Acad Sci USA 1998;95:12352–12357.
4. Ralph SA, Van Dooren GG, Waller RF, Crawford MJ, Fraunholz MJ, Foth BJ, Tonkin CJ, Roos DS, McFadden GI. Tropical infectious diseases: Metabolic maps and functions of the Plasmodium falciparum apicoplast. Nat Rev Microbiol 2004;2:203–216.
5. Nassoury N, Fritz L, Morse D. Circadian changes in ribulose-1,5-bisphosphate carboxylase/oxygenase distribution inside individual chloroplasts can account for the rhythm in dinoflagellate carbon fixation. Plant Cell 2001;13:923–934.
6. Nassoury N, Cappadocia M, Morse D. Plastid ultrastructure defines the protein import pathway in dinoflagellates. J Cell Sci 2003;116:2867–2874.
7. Hofmann E, Wrench PM, Sharples FP, Hiller RG, Welte W, Diederichs K. Structural basis of light harvesting by carotenoids: peridinin-chlorophyll-protein from *Amphidinium carterae*. Science 1996;272:1788–1791.
8. Bush KJ, Sweeney BM. The activity of ribulose diphosphate carboxylase in extracts of *Gonyaulax polyedra* in the day and the night phases of the circadian rhythm of photosynthesis. Plant Physiol 1972;50:446–451.
9. Schmitter R. The fine structure of *Gonyaulax polyedra*, a bioluminescent marine dinoflagellate. J Cell Sci 1971;9:147–173.
10. Rensing L, Taylor WR, Dunlap J, Hastings JW. The effects of protein synthesis inhibitors on the *Gonyaulax* clock II: the effect of cycloheximide on ultrastructural parameters. J Comp Physiol 1980;138:9–18.
11. Herman EM, Sweeney BM. Circadian rhythm of chloroplast ultrastructure in Gonyaulax polyedra, concentric organization around a central cluster of ribosomes. J Ultrastruct Res 1975;50:347–354.
12. Seo KS, Fritz L. Cell ultrastructural changes correlate with circadian rhythms in *Pyrocystis lunula*. J Phycol 2000;36:351–358.
13. Morse D, Salois P, Markovic P, Hastings JW. A nuclear encoded form II rubisco in dinoflagellates. Science 1995;268:1622–1624.
14. Whitney S, Andrews T. The CO_2/O_2 specificity of single-subunit ribulose-bisphosphate carboxylase from the dinoflagellate *Amphidinium carterae*. Aust J Plant Physiol 1998;25:131–138.
15. Taylor W, Krasnow T, Dunlap JC, Broda H, Hastings JW. Critical pulses of anisomycin drive the circadian oscillator in Gonyaulax towards its singularity. J Comp Physiol B 1982;148:11–25.
16. Olesiak W, Ungar A, Johnson CH, Hastings JW. Are protein synthesis inhibition and phase shifting of the circadian clock in Gonyaulax correlated? J Biol Rhythms 1987;2:121–138.
17. Helms JB, Rothman JE. Inhibition by brefeldin A of a Golgi membrane enzyme that catalyses exchange of guanine nucleotide bound to ARF. Nature 1992;360:352–354.
18. Mossessova E, Corpina RA, Goldberg J. Crystal structure of ARF1*Sec7 complexed with brefeldin A and its implications for the guanine nucleotide exchange mechanism. Mol Cell 2003;12:1403–1411.
19. Dascher C, Balch WE. Dominant inhibitory mutants of ARF1 block endoplasmic reticulum to Golgi transport and trigger disassembly of the Golgi apparatus. J Biol Chem 1994;269:1437–1448.
20. de Lanerolle P, Cole AB. Cytoskeletal proteins and gene regulation: form, function, and signal transduction in the nucleus. Sci STKE 2002; PE30.
21. Torii S, Banno T, Watanabe T, Ikehara Y, Murakami K, Nakayama K. Cytotoxicity of brefeldin A correlates with its inhibitory effect on membrane binding of COP coat proteins. J Biol Chem 1995; 270: 11574–11580.
22. Coppens I, Andries M, Liu JL, Cesbron-Delauw MF. Intracellular trafficking of dense granule proteins in Toxoplasma gondii and experimental evidences for a regulated exocytosis. Eur J Cell Biol 1999;78: 463–472.
23. McDougall C. Bioluminescence and the actin cytoskeleton in the dinoflagellate *Pyrocystis Fusiformis*: an examination of organelle transport and mechanotransduction. (PhD Thesis). Santa. Barbara: University of California; 2002.
24. Orci L, Perrelet A, Ravazzola M, Wieland FT, Schekman R, Rothman JE. "BFA bodies": a subcompartment of the endoplasmic reticulum. Proc Natl Acad Sci USA 1993;90:11089–11093.
25. Bertomeu T, Morse D. Isolation of a dinoflagellate mitotic cyclin by functional complementation in yeast. Biochem Biophys Res Commun 2004;323:1172–1183.
26. Rowan R, Whitney SM, Fowler A, Yellowlees D. Rubisco in marine symbiotic dinoflagellates: form II enzymes in eukaryotic oxygenic phototrophs encoded by a nuclear multigene family. Plant Cell 1996;8:539–553.
27. Zhang H, Lin S. Complex gene structure of the form II Rubisco in the dinoflagellate *Prorocentrum minimum* (Dinophyceae). J Phycol 2003;39:1160–1171.
28. Enomoto T, Sulli C, Schwartzbach SD. A soluble chloroplast protease processes the Euglena polyprotein precursor to the light harvesting chlorophyll a/b binding protein of Photosystem II. Plant Cell Physiol 1997;38:743–746.
29. Skop AR, Bergmann D, Mohler WA, White JG. Completion of cytokinesis in C. elegans requires a brefeldin A-sensitive membrane accumulation at the cleavage furrow apex. Curr Biol 2001;11:735–746.
30. Morse D, Sassone-Corsi P. Time after time: inputs to and outputs from the mammalian circadian oscillators. Trends Neurosci 2002;25: 632–637.
31. Jordan D, Ogren W. Species variation in the specificity of ribulose biphosphate carboxylase/oxygenase. Nature 1981;291:513–515.
32. Markovic P, Roenneberg T, Morse D. Phased protein synthesis at several circadian times does not change protein levels in *Gonyaulax*. J Biol Rhythms 1996;11:57–67.
33. Nassoury N, Morse D. Protein targeting to the chloroplasts of photosynthetic eukaryotes: getting there is half the fun. Biochim Biophys Acta 2005;1743:5–19.
34. Sulli C, Fang Z, Muchhal U, Schwartzbach SD. Topology of Euglena chloroplast protein precursors within endoplasmic reticulum to Golgi to chloroplast transport vesicles. J Biol Chem 1999;274:457–463.
35. Tarricone C, Xiao B, Justin N, Walker PA, Rittinger K, Gamblin SJ, Smerdon SJ. The structural basis of Arfaptin-mediated cross-talk between Rac and Arf signalling pathways. Nature 2001; 411:215–219.
36. Dunlap JC, Taylor WR, Hastings JW. The effects of protein synthesis inhibitors on the Gonyaulax clock I: phase shifting effects of cycloheximide. J Comp Physiol 1980;138:1–8.
37. McMurry L, Hastings JW. No desynchronization among the four circadian rhythms in the unicellular alga, *Gonyaulax polyedra*. Science 1972; 175:1137–1139.
38. Bode VC, DeSa R, Hastings JW. Daily rhythm of luciferin activity in *Gonyaulax polyedra*. Science 1963;141:913–915.
39. Morse D, Milos PM, Roux E, Hastings JW. Circadian regulation of bioluminescence in *Gonyaulax* involves translational control. Proc Natl Acad Sci USA 1989;86:172–176.
40. Dunlap JC, Hastings JW. The biological clock in *Gonyaulax* controls luciferase activity by regulating turnover. J Biol Chem 1981; 256: 10509–10518.
41. Johnson CH, Roeber J, Hastings JW. Changes in luciferase amount account for the circadian bioluminescece rhythm in Gonyaulax. Science 1984, 1428–1430.

42. Mittag M, Lee D-H, Hastings JW. Circadian expression of the luciferin-binding protein correlates with the binding of a protein to the 3′ untranslated region of its mRNA. Proc Natl Acad Sci USA 1994;91:5257–5261.
43. Fritz L, Morse D, Hastings JW. The circadian bioluminescence rhythm of *Gonyaulax* is related to daily variations in the number of light-emitting organelles. J Cell Sci 1990;95:321–328.
44. Nicolas MT, Morse D, Bassot JM, Hastings JW. Colocalization of luciferin binding protein and luciferase to the scintillons of *Gonyaulax polyedra* revealed by double immunolabeling after fast freeze fixation. Protoplasma 1991;160:159–166.
45. Guillard RRL, Ryther JH. Studies on marine planktonic diatoms: *Cyclotella nana* Hufstedt and *Denotula confervacea* (Cleve) Gran. Can J Microbiol 1962;8:229–239.
46. Crutchfield ALM, Diller KR, Brand JJ. Cryopreservation of *Chlamydomonas reinhardtii* (Chlorophyta). Eur J Phycol 1999; 34:43–52.